The Cryosphere

Discussions

Open Access

EGU

Large and irreversible future decline of the Greenland ice-sheet

Jonathan M. Gregory[1,2,*], Steven E. George[1,*], and Robin S. Smith[1,*]

[1]National Centre for Atmospheric Science, University of Reading, UK
[2]Met Office Hadley Centre, Exeter, UK
[*]All authors made essential contributions to this work.

Correspondence: Jonathan Gregory (j.m.gregory@reading.ac.uk)

Abstract.

We have studied the evolution of the Greenland ice-sheet under a range of constant climates typical of those projected for the end of the present century, using a dynamical ice-sheet model (Glimmer) coupled to an atmospheric general circulation model (FAMOUS-ice AGCM). The ice-sheet surface mass balance (SMB) is simulated by the AGCM, including its dependence on

5   altitude within AGCM gridboxes. Over millennia under a warmer climate, the ice-sheet reaches a new steady state, whose mass is correlated with the initial perturbation in SMB, and hence with the magnitude of global climate change imposed. For the largest global warming considered (about +5 K), the contribution to global-mean sea-level rise (GMSLR) is initially 2.7 mm yr^{-1}, and the ice-sheet is eventually practically eliminated (giving over 7 m of GMSLR). For all RCP8.5 climates, final GMSLR exceeds 4 m. If recent climate were maintained, GMSLR would reach 1.5–2.5 m. Contrary to expectation from earlier

10   work, we find no evidence for a threshold warming that divides scenarios in which the ice-sheet suffers little reduction from those which it is mostly lost. This is because the dominant effect is reduction of area, not reduction of surface altitude, and the geographical variation of SMB must be taken into account. The final steady state is achieved by withdrawal from the coast in some places, and a tendency for increasing SMB due to enhancement of cloudiness and snowfall over the remaining ice-sheet, through the effects of topographic change on atmospheric circulation. If late twentieth-century climate is restored, the ice-sheet

15   will not regrow to its present extent, owing to such effects, once its mass has fallen below a threshold of about 4 m of sea-level equivalent. In that case, about 2 m of GMSLR would become irreversible. In order to avoid this outcome, anthropogenic climate change must be reversed before the ice-sheet has declined to the threshold mass, which would be reached in about 600 years at the highest rate of mass-loss within the likely range of the Fifth Assessment Report of the Intergovernmental Panel on Climate Change.

1 Introduction

1.1 Mass-loss from the Greenland ice-sheet in recent decades

During 1961–1990 the Greenland ice-sheet had a roughly constant mass, in which snow accumulation P was balanced by the sum of surface ablation R (meaning all processes of mass-loss, predominantly liquid runoff due to melting) and solid discharge

25 D of ice into the sea (forming icebergs). Over the last 30 years both R and D have increased significantly while P has not, giving a current rate of mass-loss of about $250 \, \mathrm{Gt \, yr^{-1}}$, or $0.7 \, \mathrm{mm \, yr^{-1}}$ sea level equivalent (SLE) (Shepherd et al., 2012; van den Broeke et al., 2016; Bamber et al., 2018; Mouginot et al., 2019). This accounts for about 20% of global-mean sea-level rise (GMSLR) of recent years, most of which is due to thermal expansion of seawater (*i.e.* thermosteric) or mass-loss from glaciers.

30 The increase in D is probably the ice-dynamical response of outlet glaciers to reduced buttressing by their ice-tongues, which have thinned due to basal melting by warmer sea-water (Holland et al., 2008). Although ice discharge is projected to increase in coming decades with rising water temperature, it will decline on longer timescales as the ice-sheet thins at the coast and its outlet glacier termini retreat inland (Nick et al., 2013; Fürst et al., 2015; Aschwanden et al., 2019).

The increase in R causes 60% of the mass-loss (van den Broeke et al., 2016; Fettweis et al., 2017). It has been partly due

35 to anthropogenic climatic warming, which is amplified at high northern latitudes, and partly to recent unusual atmospheric circulation (Tedesco et al., 2013; Fettweis et al., 2017; Pattyn et al., 2018; Trusel et al., 2018). The surface mass balance (SMB $S = P - R$, the net addition of mass) in recent years has fallen lower than during the warm period in Greenland in the early twentieth century (Fettweis et al., 2017) and summer temperatures have risen higher (Hanna et al., 2012). Some recent summers have seen surface melting over practically the entire ice-sheet because of high air temperature, decreased cloudiness

40 and reduction of albedo, the latter due to the increase of snow grain size and the exposure of bare ice, both caused by surface snow melting (Tedesco et al., 2013, 2016; Hofer et al., 2017; Trusel et al., 2018).

1.2 Projections of future mass-loss

The future of the Greenland ice-sheet is one of the large uncertainties in projections of GMSLR (Church et al., 2013; Clark et al., 2016). Projections indicate that R will increase non-linearly with temperature and more rapidly than P, meaning that

45 SMB will continue to decline and the rate of mass-loss will grow, especially under scenarios of high CO_2 emissions (Gregory and Huybrechts, 2006; Fettweis et al., 2013; Vizcaíno et al., 2014; Pattyn et al., 2018; Rückamp et al., 2018; Golledge et al., 2019; Aschwanden et al., 2019). Recent projections of the contribution of the Greenland ice-sheet to GMSLR mostly lie within the likely ranges of the Fifth Assessment Report (AR5) of the Intergovernmental Panel on Climate Change (Church et al., 2013) *viz.* 0.04–0.12 m and 0.09-0.28 m by 2100 relative to 1986–2005 under scenarios RCP2.6 and RCP8.5 respectively. The

50 range of uncertainty arises from the model spread in amplification of warming in Greenland relative to global warming, as well as the sensitivity of Greenland SMB to regional climate change (Gregory and Huybrechts, 2006; Fettweis et al., 2013). Although substantial, these contributions are only 10–30% of projected GMSLR.

The importance of the Greenland ice-sheet is greater on multicentury timescales, because its size (mass $M = 7.4$ m SLE) implies a large commitment to GMSLR. Thinning of the ice-sheet due to positive ΔR (Δ denoting the difference from the initial state) is affected by a positive feedback loop between SMB and elevation: as the surface elevation falls, the surface air temperature rises, and surface melting increases, magnifying ΔR. Another positive feedback on ΔR is caused by the decrease in surface albedo due to melting, as in recent years (Tedesco et al., 2016). Despite the feedbacks, a steady state could be regained with an ice-sheet of smaller mass but little loss of area if the reduction of SMB were compensated by the reduction of discharge resulting from thinning of outlet glaciers (Rückamp et al., 2018). The reduction of mass would be mitigated if $\Delta P > 0$, as projected by GCMs.

On the other hand, previous work indicates there may be a threshold T_c of global-mean surface air temperature change ΔSAT (relative to pre-industrial) beyond which the ice-sheet will vanish (Huybrechts et al., 1991; Gregory et al., 2004; Gregory and Huybrechts, 2006; Robinson et al., 2012) (see Section 2). Levermann et al. (2013) estimated $T_c = 0.8$–2.2 K, using the model of Robinson et al. (2012) constrained by information from the last interglacial (Robinson et al., 2011). If this range is correct, limiting ΔSAT to 2.0 K in accordance with the Paris agreement or to its aspiration of 1.5 K could make a critical difference to whether T_c is exceeded (Pattyn et al., 2018). Loss of the Greenland ice-sheet would cause much greater GMSLR than from glacier mass-loss or thermosteric sea-level rise for similar degrees of warming (Church et al., 2013; Levermann et al., 2013) although, even in the most extreme scenarios, the complete removal of the ice-sheet would take a least a thousand years (*e.g.* Ridley et al., 2005; Aschwanden et al., 2019).

1.3 Possibility of irreversible mass-loss

Because of the elevation and albedo feedbacks, SMB might remain negative in some deglaciated regions after CO_2 fell and the climate cooled, meaning that the present ice-sheet could not be regenerated in pre-industrial climate (Toniazzo et al., 2004), and may actually be a relict of a colder climate (Solgaard et al., 2013). This implies the existence of two steady states of the ice-sheet (either absent, or present as now) in pre-industrial climate. Previous work shows there may be more than two (Charbit et al., 2008; Ridley et al., 2010; Solgaard and Langen, 2012; Robinson et al., 2012). Stable states of intermediate size are possible because of the interaction of the ice-sheet with its own climate through atmospheric dynamics, whereby its surface topography affects regional precipitation and temperature, like mountains do. The existence of intermediate states means that partial loss of the ice-sheet could be irreversible.

It is the possibility of threshold behaviour (*i.e.* "tipping-points") and irreversibility which makes the future of the Greenland ice-sheet of particular concern (Pattyn et al., 2018). Precautionary action to mitigate the threat of irreversible damage is a principle of the Framework Convention of Climate Change (Article 3.3), even when there is not full scientific certainty. The serious implications of the uncertainty are the motivation for the work presented in this paper, in which we reexamine the future decline and possible recovery of the ice-sheet. Previous work on the subject has used simplified climate models, or a small set of climate states, or been limited to a few centuries into the future. In the present work we use a dynamic ice-sheet model coupled to a atmosphere general circulation model (AGCM) to study the transient and steady states of the ice-sheet over tens of millennia. Our conclusions differ in some critical ways from those of previous work.

2 Conceptual basis for the existence of a threshold warming

The rate of change of the mass of the ice-sheet is $\mathrm{d}M/\mathrm{d}t = S - D$. In the unperturbed steady state $\mathrm{d}M/\mathrm{d}t = 0 \Rightarrow S = D$ *i.e.* SMB S is balanced by discharge D. In a warmer climate, ablation R and snowfall P both increase, but $\Delta R > \Delta P \Rightarrow \Delta S = \Delta P - \Delta R < 0$. A new steady state can be achieved if $\Delta D = \Delta S$ *i.e.* if discharge reduces by as much as SMB.

Let us suppose that changing the global-mean SAT by T initially perturbs the ice-sheet area-mean specific SMB s by an amount $\Delta s(T)$. Specific SMB is the excess of snowfall over ablation at a location, and its area-integral is the quantity we usually call just "SMB" *i.e.* $S = As$, where A is ice-sheet area. The initial change in SMB is $\Delta S = A \Delta s(T)$. Further suppose that a new steady state can be achieved by marginal thinning of the ice-sheet, which will reduce D with little change in A. However the elevation and albedo feedbacks may amplify the (negative) change in specific SMB, and require $\Delta D = \Delta S = A\Delta s(T)(1 + f(\Delta M))$ in the reduced steady state, where f is a function representing the feedbacks, with $f(0) = 0$ initially, and f increasing as ΔM becomes more negative.

This argument leads to the idea of a threshold T_c that gives a steady state with a loss ΔM_c of mass, such that $\Delta S = A\Delta s(T_c)(1 + f(\Delta M_c)) = -S$, in which SMB and D are both reduced to zero ($S + \Delta S = 0$, with $S = D$ and $\Delta S = \Delta D$, so $D + \Delta D = 0$), the latter achieved by just sufficient marginal thinning to cause all outlet glaciers to retreat from the coast. Any T exceeding T_c will give negative SMB, but D cannot be further reduced (*i.e.* below zero) to compensate. Hence $T > T_c$ is expected to lead to the elimination of the ice-sheet by the so-called small ice-cap instability, wherein s must become increasingly negative as the surface gets lower. Therefore T_c is the greatest global warming that the ice-sheet can endure.

The threshold was estimated as 1.9–4.5 K relative to pre-industrial (Gregory and Huybrechts, 2006; Meehl et al., 2007), by assuming it equals the warming required to reduce SMB to zero with the present-day surface topography *i.e.* $\Delta S = A\Delta s(T_c) = -S$. This method overestimates T_c by neglecting the feedbacks represented by f. Although S may remain positive after the initial perturbation, it may become negative due to the feedbacks before a steady state is reached. To take $f(\Delta M)$ into account, ΔM must be predicted, for which Robinson et al. (2012) used a dynamical ice-sheet model, thus arriving at their smaller T_c.

3 Model

Typical AGCMs are not suitable for modelling ice-sheet SMB, because they do not have adequate treatments of albedo and hydrology, nor fine enough spatial resolution for the large gradients in topography and climate parameters across the margins of the ice-sheets, where much of the snowfall and snowmelt occurs (Vizcaíno, 2014). Specially developed regional climate models (RCMs) have proven very useful for high-resolution projections and process studies (*e.g.* MAR RCM, Fettweis et al., 2013; RACMO RCM, Noël et al., 2018) but they require lateral boundary conditions (BCs) from global GCMs, and cannot feed back on climate change outside their domain. Moreover, computational expense prevents the use of these RCMs in studying ice-sheet evolution over millennia.

3.1 FAMOUS–ice AGCM

For sufficient speed, we use the FAMOUS AGCM, which is the atmosphere component of the FAMOUS atmosphere–ocean general circulation model (AOGCM) (Smith et al., 2008; Smith, 2012), itself a low-resolution version, at 7.5° longitude by

120   5° latitude, of the HadCM3 AOGCM (Gordon et al., 2000). To simulate the important effects of topographic gradients and snow hydrology for ice-sheets, in this work we use "FAMOUS–ice", a new version of FAMOUS (version sgfjb, Smith et al., in preparation), incorporating a multilayer surface snow scheme which calculates melting, refreezing of meltwater, runoff and SMB on "tiles" at a set of elevations within each AGCM gridbox (each tile covering a fraction of the gridbox area). This is similar to the approach of Vizcaíno et al. (2013), and we use the same ten elevations as them.

125   For vertical interpolation of atmospheric variables from the AGCM gridbox elevation to the tile elevations we prescribe a lapse rate of $6 \, \mathrm{K \, km^{-1}}$ for air temperature. This we obtained from the climate of 1980–1999 simulated by Fettweis et al. (2013) with the MAR RCM using sea-surface BCs (sea-surface temperature and sea-ice) from MIROC5, the AOGCM which Fettweis et al. found to give the most satisfactory SMB simulation. (The same uniform lapse rate is used *e.g.* by Aschwanden et al., 2019.) Downwelling longwave radiation and specific humidity are vertically interpolated in FAMOUS–ice using gradients

130   consistent with the prescribed lapse rate, but precipitation is not redistributed vertically, nor modified in phase.

We have paid particular attention to the treatment of the surface albedo of the Greenland ice-sheet, to which SMB is very sensitive. Bare ice has lower albedo than snow in FAMOUS–ice and snow albedo has different values for visible and near-infrared, both dependent on the snow-grain size, which is a prognostic that depends on the "ageing" of the surface snow by melting and refreezing following new snowfall. There is an uncertain parameter in the relationship between snow-grain size

135   and albedo. In our experiments, we use three alternative parameter values that are consistent with observations of albedo. For convenience we refer to these as low, medium and high albedo, but the reader should keep in mind that the albedo is variable in each case. More details are given by Smith et al. (in preparation).

Instead of simulating sea surface conditions by using the FAMOUS AOGCM, we use the AGCM alone, with sea-surface BCs derived from AOGCM experiments of the Coupled Model Intercomparison Project Phase 5 (CMIP5), for both recent and

140   future climate, for two reasons. First, the FAMOUS AOGCM has larger biases in its simulation of the present-day climate than MIROC5 and the three other AOGCMs we use (CanESM2, HadGEM2-ES and NorESM1-M), which have previously been selected as satisfactory for Greenland regional climate simulation (Fettweis et al., 2013; van Angelen et al., 2013). Second, this method allows us to investigate the uncertainty in Greenland ice-sheet projections that arises from the spread of climate projections given by AOGCMs for any given scenario.

145   By prescribing sea surface conditions, we exclude any climate interaction between the ice-sheet and the ocean, in particular, possible cooling of regional climate due to weakening of the AMOC caused by meltwater from the ice-sheet (*e.g.* Vizcaíno et al., 2010). There is wide uncertainty in this aspect of ocean climate change, whose implications for the ice-sheet could possibly be explored in further work by modifying the sea-surface temperatures in a range of ways to represent the effects of AMOC changes projected by AOGCMs (Stouffer et al., 2006; Gregory et al., 2016).
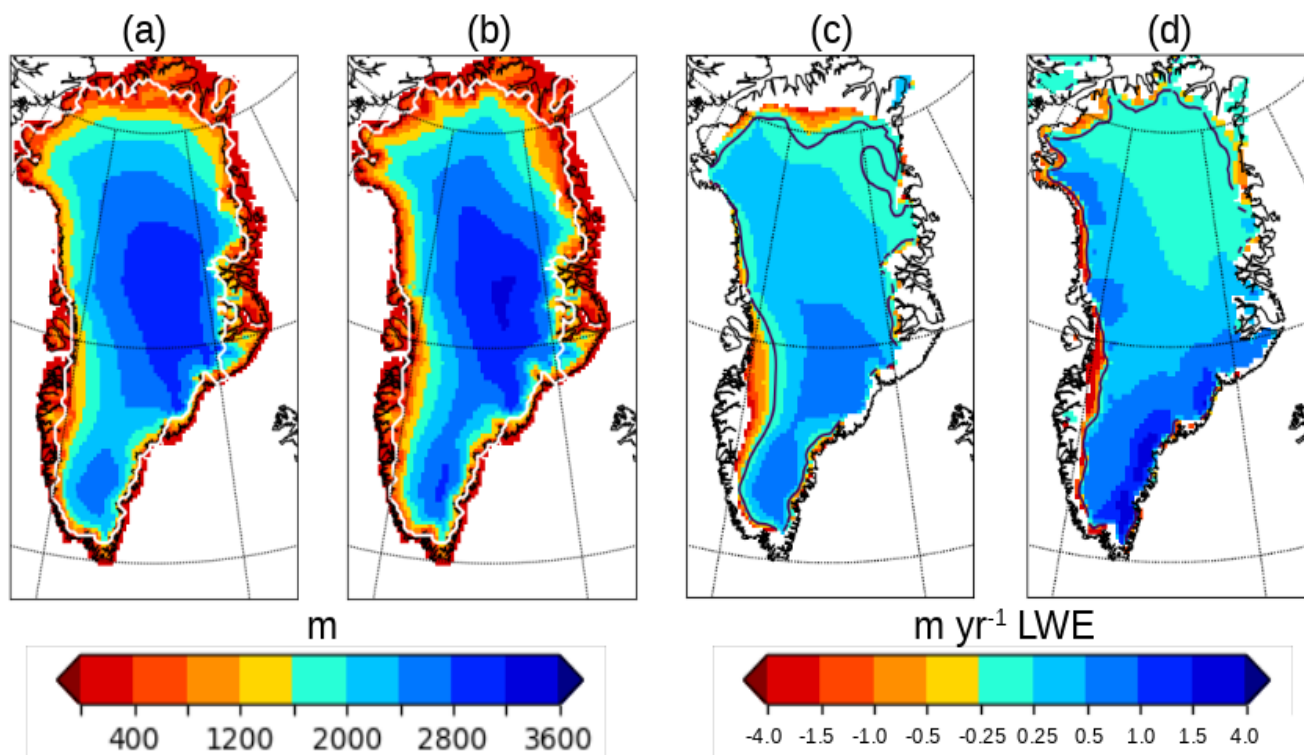
Figure 1. (a,b) Comparison of Greenland surface elevation above sea level in (a) FAMOUS–ice (medium albedo) and (b) observations (Bamber et al., 2001a, b). The white contour is the ice margin. (c,d) Comparison of specific surface mass balance (expressed as liquid water equivalent) for the climate of MIROC5 1980–1999 in (c) FAMOUS–ice (medium albedo), (d) MAR. The black contour is the equilibrium line (where specific SMB is zero).

3.2 FiG coupling and spinup

We use the Glimmer-CISM community ice-sheet model (Rutt et al., 2009, `https://cism.github.io`) with the shallow-ice approximation at 20 km grid-spacing. Because the ice-sheet model lacks sufficient resolution and physical processes to simulate calving into fjords, we instantly remove ice which flows beyond the present margin of the ice-sheet. This BC prevents a tendency for the ice-sheet to expand slightly, and it becomes irrelevant in most of our experiments, when the ice-sheet contracts. For simplicity in the model we omit isostatic uplift, which in reality gives a negative feedback on ice-sheet mass-loss through the elevation–SMB feedback, because it is not a large effect (*e.g.* 2% over 1000 years, Aschwanden et al., 2019) and does not seem necessary given that our scenarios are idealised in other ways as well.

The AGCM and the ice-sheet model are coupled to make FAMOUS–ice–Glimmer (FiG, Gregory et al., 2012; Roberts et al., 2014; Smith et al., in preparation). After each AGCM year, the SMB simulated by the AGCM is interpolated horizontally

160 and vertically (with the AGCM tile elevation as the vertical coordinate) to the ice-sheet surface topography, and the AGCM topography and land-surface properties are updated according to the ice-sheet model. FiG runs at about 220 simulated AGCM years per wallclock day on six cores, with the AGCM consuming the great majority of the CPU time. Although this is fast for a GCM, it is not fast enough for multimillennial experiments, so we run 10 years of the ice-sheet model using each AGCM year's SMB, depending on the assumption that the elevation–SMB feedback will be negligible for changes in topography that

165 occur within a decade. We have verified that this 10:1 acceleration makes no significant difference to our results. Hereafter by "year" in FiG experiments we mean an ice-sheet year except where otherwise stated.

Because our aim is to simulate ice-sheet response to climate change over millennia, we have to start from a coupled steady state, with little long-term tendency in the ice-sheet topography. We initiate the ice-sheet model with observed topography (Bamber et al., 2001a, b) and run FiG under the MIROC5 AOGCM climate of 1980–1999, during which period the ice-sheet

170 was near to a steady state in reality (van den Broeke et al., 2016). In the first millennium the ice-sheet mass M increases by 0.1–0.2 m SLE. With medium and low albedo it subsequently decreases again more slowly, while with high albedo it continues to grow slowly and stabilises after 4 kyr at 0.3 m SLE above present-day (Figure A1). The states obtained after about 4 kyr of spin-up are used to initiate the experiments described in Section 4. In these states M is close to reality, and the topography similar to observed (Figure 1a,b), with the summit and southern dome altitudes being a few 100 m too low. (See

175 also Appendix A concerning the constraint implied on albedo by the requirement of realistic M.)

3.3   Simulated surface mass balance

Comparing the three choices of albedo in FAMOUS–ice with BCs for the MIROC5 1980–1999 climate, we find that lower albedo produces lower SMB (the first group of cases in Table 1 differ significantly at the 10% level), because ablation is greater due to greater snowmelt, but snowfall is about the same (slightly larger with higher albedo because of greater ice-sheet area).

180 For the same albedo (medium), the SMB is significantly lower with the CanESM2 and NorESM1-M historical climates than with MIROC5 because the ablation is larger, whereas the SMB is about the same with HadGEM2-ES as with MIROC5 (the second group in the table). This shows the influence of the different climate simulations of the AOGCMs.

However, comparison of FAMOUS–ice with MAR and RACMO for the same climates shows that the formulation of the regional climate model is at least as influential as the choice of climate BCs. MAR gives much larger SMB than FAMOUS–

185 ice with the MIROC5 climate, because of smaller ablation, while RACMO gives larger ablation than FAMOUS–ice with the HadGEM2-ES climate (the third group in the table). Comparison with MAR and RACMO for ERA-interim BCs (*i.e.* observationally derived, the fourth group in the table) suggests that FAMOUS–ice with high albedo is similar to both of them.

Regarding its geographical distribution, FAMOUS–ice SMB interpolated to the Glimmer grid compares favourably with the MAR simulation for the MIROC5 climate (Figure 1c,d). It shows positive and negative values of realistic magnitude, and

190 reproduces the important geographical features, including the confinement of negative SMB to the margins, especially on the west coast, the decrease in positive SMB towards the north-east, and the occurrence of greatest positive SMB in the strip of maximum snowfall along the south-east coast. We presume that the latter is not sufficiently intense in FAMOUS–ice because of the low resolution of the AGCM. The equilibrium line altitude is similar in the two models (black contour).

Climate	Greenland model (albedo)	SMB	Snowfall	Ablation
1980-1999 climates				
MIROC5	FAMOUS–ice (low)	310 ± 10	693	383
MIROC5	FAMOUS–ice (medium)	332 ± 11	697	364
MIROC5	FAMOUS–ice (high)	414 ± 9	715	300
CanESM2	FAMOUS–ice (medium)	272 ± 21	681	409
HadGEM2-ES	FAMOUS–ice (medium)	312 ± 20	705	393
NorESM1-M	FAMOUS–ice (medium)	287 ± 16	721	434
MIROC5	MAR	437 ± 24	681	244
CanESM2	MAR	410 ± 23	635	225
HadGEM2-ES	RACMO	244 ± 25	660	416
NorESM1-M	MAR	483 ± 16	691	208
ERA-interim	MAR	388 ± 23	637	249
ERA-interim	RACMO	406 ± 22	683	277
MIROC5 2080-2099 climates				
RCP2.6	FAMOUS–ice (medium)	325 ± 14	704	379
RCP4.5	FAMOUS–ice (medium)	150 ± 25	735	585
RCP8.5	FAMOUS–ice (medium)	-207 ± 35	805	1013

Table 1. Greenland area-integral surface mass balance (SMB), snowfall and ablation (all in $\mathrm{Gt\,yr^{-1}}$) for FAMOUS–ice with MIROC5 AOGCM historical climate (with the three choices of FAMOUS–ice albedo), FAMOUS–ice with historical climates of other AOGCMs (FAMOUS–ice medium albedo only), the MAR and RACMO RCMs with the same AOGCM climates and with ERA-interim climate (from Table 2 of Fettweis et al., 2013), and FAMOUS–ice with MIROC5 AOGCM climate (medium albedo only) under RCP scenarios. Ablation is SMB $-$ snowfall, mainly runoff from snowelt, and including evaporation, sublimation, condensation and rainfall freezing in the snowpack (in the RCMs; all rainfall runs off in FAMOUS–ice). The $\pm$ uncertainty shown for SMB is the standard error of the time-mean, estimated by assuming annual values to be independent. The SMB from FAMOUS–ice has smaller standard errors than from the RCMs for two reasons. First, the FAMOUS–ice integrations exclude interannual variability due to SST and sea-ice by using climatological mean BCs. Second, the RCM time-means use 20 years of data, while we use 30 years from the second group of FAMOUS–ice simulations, and 100 from the first.

CMIP5 scenario	years	CO_2	ERF	notes
historical	1980-1999	402	2.1	
RCP2.6	2080–2099	402	2.1	
RCP4.5	2080-2099	650	4.7	
RCP8.5	2080–2099	1200	8.0	not with HadGEM2-ES
abrupt4xCO2	121–140	1200	8.0	CanESM2 and low albedo only
abrupt4xCO2	101–120	1200	8.0	HadGEM2-ES and low albedo only

Table 2. AOGCM climates used to supply sea-surface boundary conditions for the first set of FiG experiments. The BCs mostly determine the climate, while the CO_2 concentration (in ppm) has a relatively small influence. For simplicity only three different CO_2 concentrations were used, chosen to give approximately the nominal effective radiative forcing (ERF, $W\,m^{-2}$) of the RCPs, and all other forcing agents were as pre-industrial.

4   Mass-loss of the ice-sheet in warmer climates

We run a set of 47 FiG experiments to study the SMB change (ΔSMB), rate of mass-loss and eventual steady state of the Greenland ice-sheet, using the three different choices of FAMOUS–ice snow-albedo parameter, with 20-year climatological monthly mean sea-surface BCs taken from the four selected CMIP5 AOGCMs for five climate scenarios (Table 2). These five are the recent past (1980–1999, called "historical"), the end of the 21st century under three RCP scenarios (representative concentration pathway, as in the AR5; van Vuuren et al., 2011), and quadrupled pre-industrial CO_2 (abrupt4xCO2, warmer than any RCP). The experiments have steady-state climates. This is unrealistic, but it simplifies the comparison, and is reasonable since no-one can tell how climate will change over millennia into the future. Our simulations should be regarded only as indicative, rather than as projections.

Each experiment begins from the FiG spun-up state for MIROC5 historical climate with the appropriate albedo parameter. Although in most cases there is a substantial instantaneous change in BCs when the experiment begins, the land and atmosphere require only a couple of years to adjust. Being climatological means, the sea-surface BCs lack interannual variability, and we have checked that statistically indistinguishable results for the ice-sheet are obtained by cycling through a 20-year series of monthly mean BCs.

4.1   Evolution of surface mass balance

Our set of BCs produces a wide range of global mean surface air temperature change ΔSAT of -1 to $+5$ K, relative to the MIROC5 historical climate. Some are negative because the historical climate is warmer in MIROC5 than in the other three AOGCMs. In warmer climates, snowfall and ablation are both increased (Table 1 for MIROC5 with medium albedo). In general, the greater the global warming, the more negative the ΔSMB initially produced, relative to the time-mean historical state with the same albedo (Figure 2a).

The greatest global warming is given by HadGEM2-ES abrupt4xCO2. With low albedo, this climate produces the most

215   negative ΔSMB, of $-1063\,\mathrm{Gt\,yr^{-1}}$ (it changes from $+307$ to $-756\,\mathrm{Gt\,yr^{-1}}$) in the time-mean of the first 300 years, during

which the topography hardly changes from its initial state (Figure 3a1,b1). Although this is a large perturbation, the ΔSMB of

Aschwanden et al. (2019) for RCP8.5 is larger still, perhaps because they use a degree-day scheme and assume geographically

uniform warming.

In our experiment, the specific SMB is strongly negative all around the margin and especially in the southern dome, where it

220   has a local maximum in the historical climate (Figure 3a2,b2). The snowfall on the ice-sheet is 10% larger in the abrupt4xCO2

climate (Figures 3a4,b4). We note that the precipitation is 50% larger, consistent with the warming in Greenland of 11 K and

the increase of $\sim$5% $\mathrm{K^{-1}}$ found by previous studies *e.g.* Gregory and Huybrechts (2006), but the snow fraction declines from

88% to 67%. The downwelling surface shortwave radiation in summer (June–August) is smaller because cloudiness is greater

(Figures 3a3,b3). Both the increased snowfall and the reduced insolation tend to make ΔSMB positive, but ΔSMB is actually

225   large and negative because of the overwhelming effect of increased downwelling surface longwave radiation, which is mainly

due to the air above the ice-sheet being warmer, and partly to the increase in cloud cover.

We find that the relationship between ΔSAT and ΔSMB in the set of FiG experiments roughly follows the cubic formula

(shown as the solid curve in Figure 2a) derived by Fettweis et al. (2013) for MAR projections and used in the AR5 for the

Greenland contribution to GMSLR. There is a small spread due to the choice of albedo parameter, and a larger spread due to

230   the AOGCM-dependent relationship between ΔSAT and Greenland climate change. The FiG ΔSMB mostly lies within the

AR5 likely range (dashed curves). In the majority of cases SMB remains positive (Figure 2b), but because the ice-sheet was

initially in balance, negative ΔSMB leads to loss of mass (Figure 4a). In the most extreme case, rapid retreat of the ice-sheet

---

Figure 2 *(following page).* Relationships between various quantities in the first set of experiments, with FiG under constant climates listed in Table 2, and run to a steady state, as shown in Figure 4b. All panels use the key of (a) for colours; (b–e) use the key of (a) for symbols. (a) Time-mean ΔSMB *vs.* ΔSAT, both for the first 300 years relative to the initial steady state under the historical MIROC5 climate with the same albedo parameter. The solid curve is the cubic relationship fitted by Fettweis et al. (2013) to MAR projections, and the dashed curves delimit the likely range of the AR5. (b) Trajectories of ice-sheet SMB (not ΔSMB) *vs.* mass M, shown as 200-year means for the first millennium, and 1000-year means thereafter. The trajectories begin at the symbols, with M close to the observed for the present day, and a wide range of SMB. They end with a wide range of M, but all have positive SMB. (c) Final steady-state M *vs.* time-mean ΔSAT in FAMOUS–ice for the first 300 years. (d) Final steady-state M of the ice-sheet *vs.* time-mean ΔSMB of the first 300 years. The vertical dashed lines mark the observational estimates of ΔSMB for the recent periods and studies shown in the key (van den Broeke et al., 2016; Mouginot et al., 2019; Shepherd et al., in press); for van den Broeke et al. we used the steady-state SMB for 1961–1990 and the SMB trend for 1991–2015. The oblique solid and dashed lines are linear regressions of M *vs.* ΔSMB and vice-versa respectively for ΔSMB $> -700\,\mathrm{Gt\,yr^{-1}}$. The solid horizontal lines indicate the threshold of irreversibility for medium and low albedo, and the solid vertical lines translate them into ΔSMB thresholds, with uncertainty (± 2 standard deviations) shown by the grey band. (e) Trajectories of ice-sheet thickness (volume divided by area) *vs.* specific SMB for 1000-year means, beginning at the symbols. (f) Trajectories of M *vs.* ice-sheet area as grey lines, with the final configurations indicated by the symbols, and the fitted power-law relationship shown by the black line.
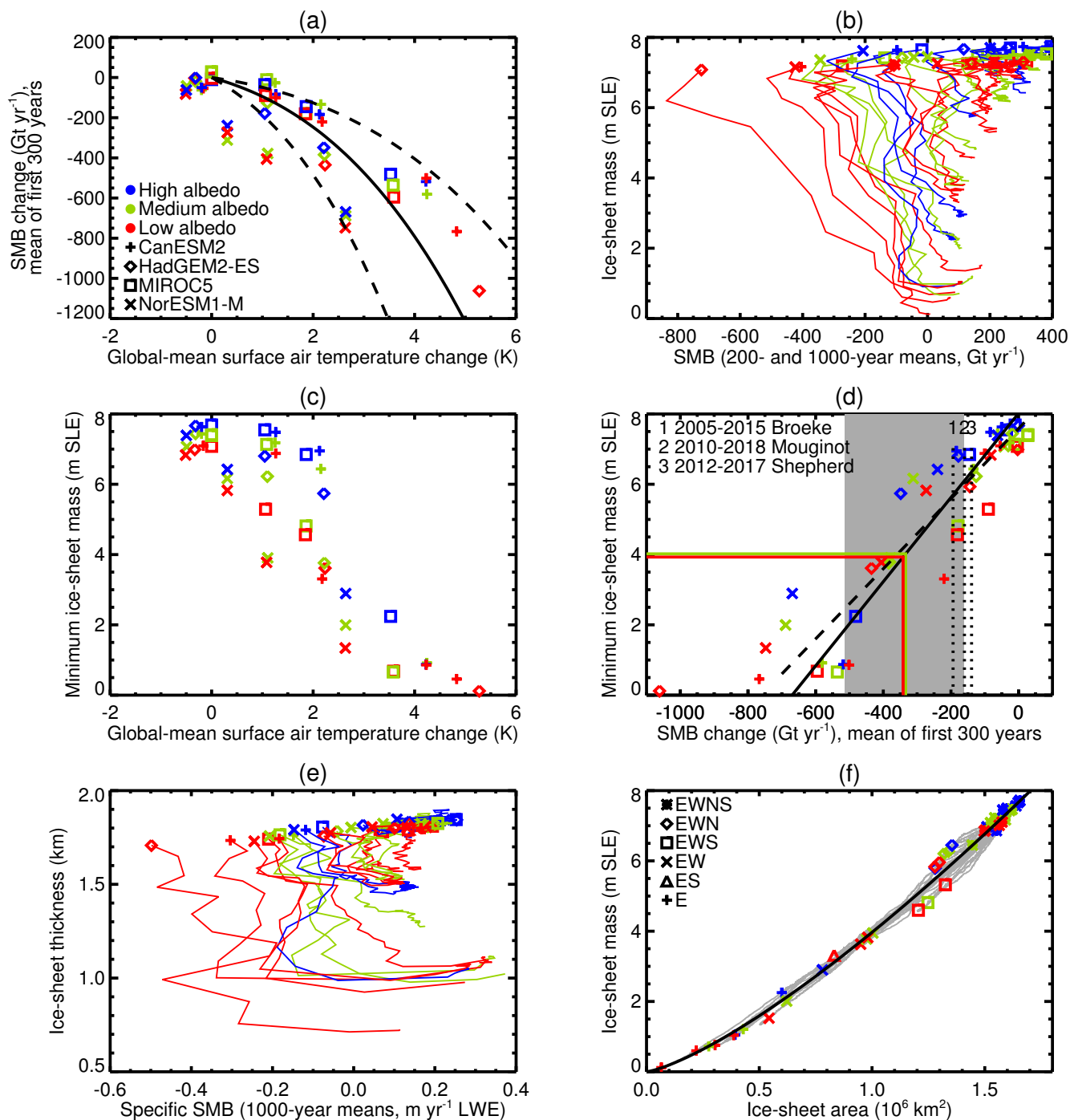
margin reduces the discharge by a third in the first century alone; this slightly offsets ΔSMB, giving ice-sheet mass-loss of 2.5 mm yr^{-1} SLE.

235   Because of the effect of lowering topography, the SMB becomes more negative in most cases during the early centuries (Figure 2b). In the 28 cases with ΔSMB < -100 Gt yr^{-1} in the time-mean of the first century, ΔSMB becomes about 20% more negative on average during the second and third centuries due to the elevation feedback, about twice the size of the effect estimated by Edwards et al. (2014) for scenario A1B by 2200. Thereafter the SMB becomes gradually more positive again (Figure 2b), because the area contracts, with the areas most prone to ablation being removed most quickly, as happens with a

240   retreating mountain glacier.

## 4.2   Final ice-sheet mass and global-mean sea-level change

The experiments continue until the ice-sheet reaches a steady state (defined as $|\mathrm{d}M/\mathrm{d}t| < 0.02$ mm yr^{-1} SLE over 2000 years). The longest experiments, which take 40 kyr (Figure 4b), are for large climate change (RCP8.5), which entails a large loss of mass, with high albedo, which causes a relatively slow rate of mass-loss. The shortest are the experiments in which a different

245   historical climate from MIROC5 is applied, because the effect on SMB of differences among AOGCMs in their simulations of recent climate is relatively minor.

There is a wide range of M in the final steady state (Figures 2b and 4b), between slightly greater than present-day (in some historical experiments), and almost zero (in abrupt4xCO2). With one exception, historical and RCP2.6 climates produce final M of 6 m SLE or more (implying GMSLR not exceeding 1.5 m), while RCP8.5 climates all produce final M of 3 m SLE

250   or less (GMSLR exceeding 4 m). In all cases the SMB is finally positive (Figure 2b), and must be balanced by ice discharge, meaning that the ice-sheet does not retreat entirely inland.

There is a clear tendency for climates of greater ΔSAT to produce smaller ice-sheets, but the final M has quite a wide range for any given initial global-mean annual-mean ΔSAT within 1–4 K (Figure 2c). For given BCs, we have found in test experiments that the ice-sheet evolution follows somewhat different trajectories from slightly different initial states, but that

255   they converge on very similar final states. Thus, the scatter in Figure 2c is not random noise, but arises from the detailed

Figure 3 *(following page)*. Illustrative states of the ice-sheet, all from coupled FAMOUS–ice–Glimmer experiments except for column (d), as follows: (a) initial steady state with HadGEM2-ES historical climate and low albedo; (b) initial state with HadGEM2-ES abrupt4xCO2 climate and low albedo; (c) transient state from the experiment of (b); (d) transient state of uncoupled Glimmer with the climate and 3D SMB of (b); (e) final state with CanESM2 abrupt4xCO2 climate and low albedo; (f) final state with MIROC5 RCP4.5 climate and medium albedo; (g,h) final states with MIROC5 historical climate and low albedo, regrown from transient states with $M = 3.83$ m SLE and $M = 4.03$ m SLE respectively in the experiment of (b). The quantity shown in each row in colours, and contour lines in rows (3–4), is stated above its colour bar. Row (1) is an instantaneous state; rows (2–4) are time-means of 30 FAMOUS–ice years, equivalent to 300 FiG years. The ice-sheet edge is shown by a thick black line in rows (2–4). The numbers in the bottom right corner are in row (1) ice-sheet mass in m SLE, (2) ice-sheet area-integral SMB in Gt yr^{-1}, (4) ice-sheet area-integral snowfall in Gt yr^{-1}. The symbols in row (1) indicate steady-state configurations by the key of Figure 2f.
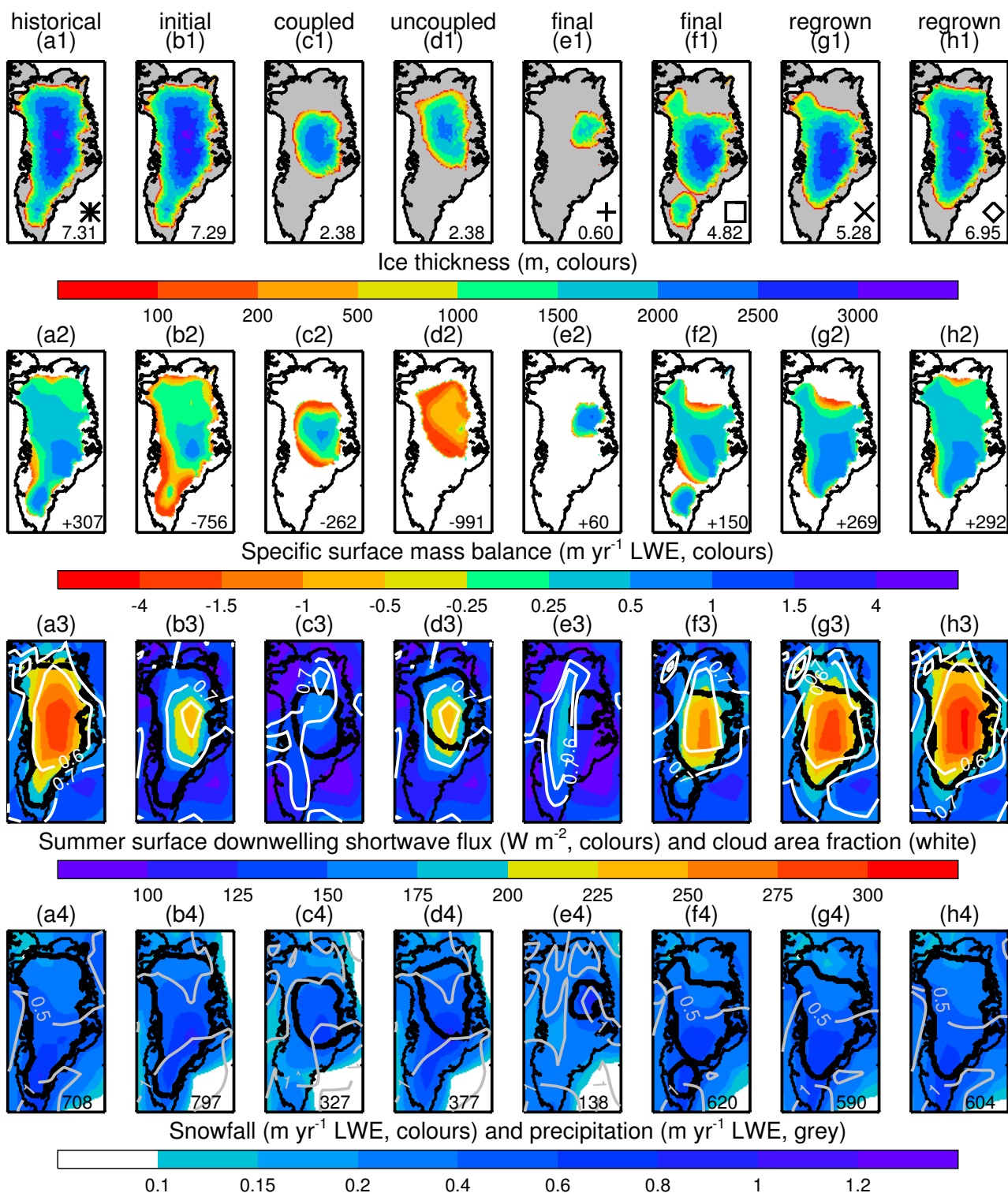
interaction of the evolving ice-sheet topography with its regional climate, which depends on the choice of BCs. The final M depends on which AOGCM is used, because of their different patterns of SST and sea-ice change; this dependence is omitted if the warming is assumed to be uniform (*e.g.* Robinson et al., 2012; Aschwanden et al., 2019).

The Pearson product–moment correlation coefficient between final M and initial ΔSAT is -0.89, and the Spearman rank correlation coefficient -0.83. The correlation is similar if for ΔSAT we use Greenland area-mean summer-mean air temperature change, either at the surface or at 600 hPa (the latter as Fettweis et al., 2013) (Figure B1). However, the relationship is better-defined using ΔSMB instead of ΔSAT (Figure 2d), with both product–moment and rank correlation coefficients of 0.92. If the initial ΔSMB is near zero, the ice-sheet changes little; the more negative the initial ΔSMB, the smaller the final M. Excluding the case with the most negative ΔSMB, a linear relationship is a fairly good fit. On the basis of the MAR simulations of Fettweis et al. (2013), the CMIP5-mean projection of ΔSMB for 2080–2099 climate is $-242\,\mathrm{Gt\,yr^{-1}}$ under RCP4.5 and $-710\,\mathrm{Gt\,yr^{-1}}$ under RCP8.5. According to the fit, the former implies eventual GMSLR of about 3 m, the latter about 7 m.

It is important to note that the spread of final M does not suggest any threshold in ΔSAT for the loss of the ice-sheet (Figure 2c). According to Section 2, there should be no final ice-sheet for negative initial SMB, implying ΔSMB below $-360\,\mathrm{Gt\,yr^{-1}}$ for FiG (Table 1), but actually there are such states (Figure 2d). This is not the picture we expected, since it is contrary to the findings of previous work, and we discuss it later (Section 5). Instead, we find that if *any* climate warmer than historical is maintained indefinitely the ice-sheet will contract to a new steady state, whose size depends on the magnitude of the warming and the consequent SMB perturbation.

Recent analyses indicate that the present ΔSMB (with respect to a steady state before the 1990s) is between -200 and $-150\,\mathrm{Gt\,yr^{-1}}$, with substantial interannual variation (*e.g.* van den Broeke et al., 2016; Mouginot et al., 2019; Shepherd et al., in press; dotted lines in Figure 2d). If a climate giving such a ΔSMB were maintained it would eventually lead to GMSLR of 1.5–2.5 m according to the linear fit (allowing for the range of FiG initial M).

4.3 Interaction of ice-sheet and climate during decline

To demonstrate the important influence of the climate–ice-sheet interaction, we repeat the HadGEM2-ES abrupt4xCO2 low-albedo experiment (the case of most negative ΔSMB) using Glimmer alone, uncoupled from the AGCM, forced by the AGCM SMB field (a function of geographical location and tile elevation) from the start of the FiG experiment. As the uncoupled experiment runs, the time-independent three-dimensional AGCM SMB field is continually interpolated onto the time-dependent ice topography using the same methods as in the FiG coupling. Thus the elevation feedback on SMB is included in the uncoupled experiment, but the feedbacks of ice-sheet topography change on the atmospheric state and circulation are excluded.

The uncoupled Glimmer and FiG experiments begin from the same initial state and have the same initial rate of mass-loss, but soon diverge (the dotted red line and the lowest solid red line in Figure 4a). While the rate of mass-loss continuously decreases in the FiG experiment, it remains almost constant (2.1–2.6 mm yr^{-1} SLE) in the uncoupled experiment for about 2.5 kyr, and the ice-sheet is completely eliminated in 3.4 kyr (Figure 4b).

To understand the different behaviour, as an example we compare the state when $M = 2.38$ m SLE, which is reached after 3600 years in the coupled experiment and 2020 years in the uncoupled. The coupled ice-sheet has a high central region
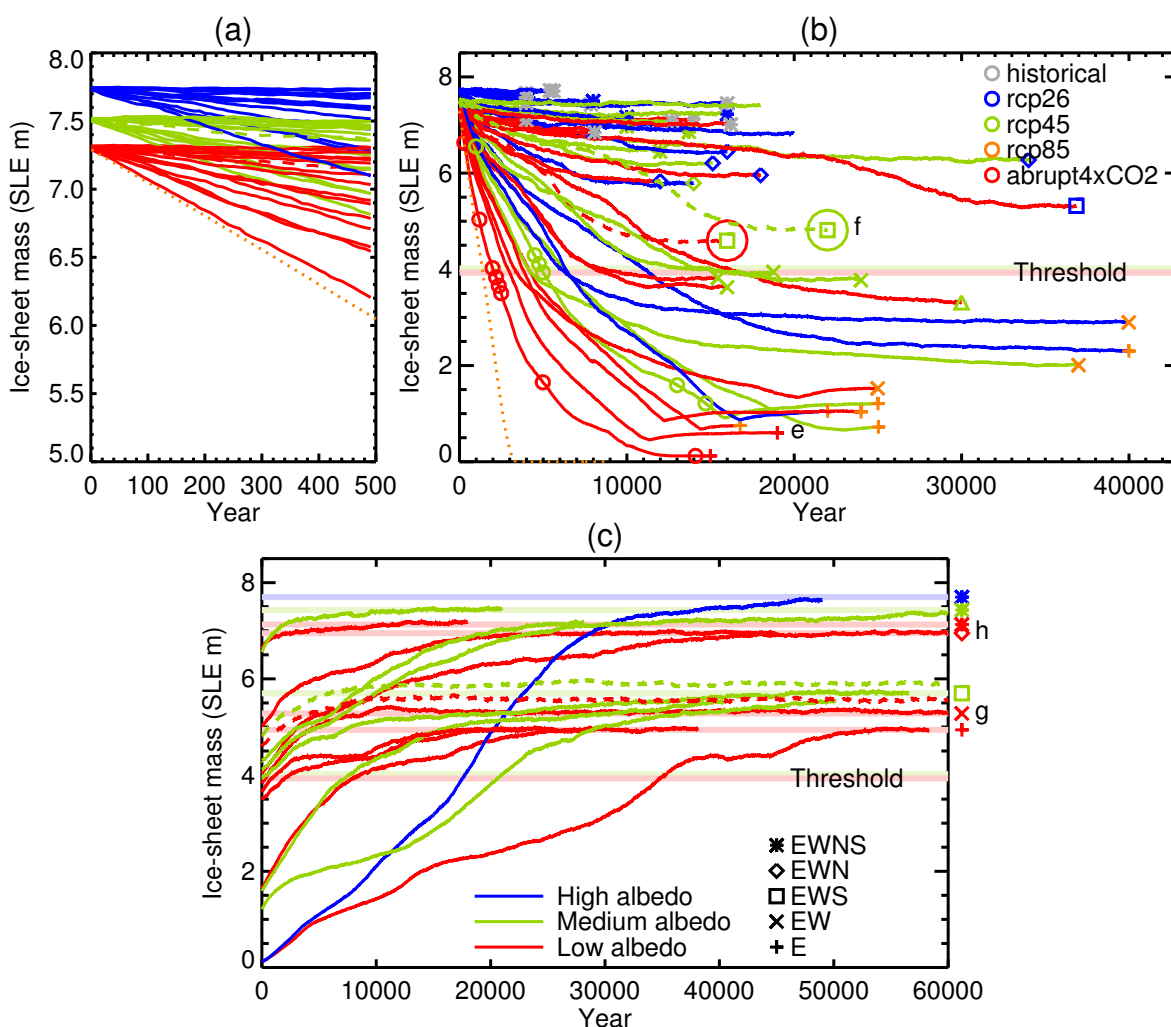
Figure 4. Timeseries of Greenland ice-sheet mass with constant climates and FAMOUS–ice albedo indicated by the line colours according to the line key of (c). (a,b) First set of experiments, beginning from steady states for MIROC5 historical (1980–1999) climate, and continuing until a new steady state is reached under the scenarios indicated by the colours of the final symbols in (b) according to its key. The solid and dashed lines are FiG experiments; the dotted line is the experiment with the uncoupled Glimmer ice-sheet model. The circles indicate transient and final states which provide the initial states for the second set of experiments. (c) Second set of FiG experiments, beginning from states of the same albedo, and continuing until a new steady state is reached under under the MIROC5 historical climate. The single high-albedo experiment begins from the low-albedo initial state of smallest mass. The experiments shown by dashed lines in (c) begin from the final states of the experiments shown by dashed lines in (b). In (b) and (c), the final symbols denote the configuration of the final steady states according to the symbol key of (c), the final states marked "e"–"h" are those shown in the columns indicated of Figure 3, and the two horizontal lines marked "Threshold" indicate the mass that divides transient states which regrow to nearly the initial steady-state mass (WOWS configurations) from those which regrow only partially (NON configurations).

290   (Figure 3c1), where specific SMB exceeds $0.25 \, \mathrm{m \, yr^{-1}}$ LWE over about the same area as in the initial state (Figure 3b2,c2), surrounded closely by steep narrow margins with large negative specific SMB, giving negative area-integral SMB which is $\sim$3 times smaller than in the initial state under 4xCO2. The regions where negative specific SMB appears were near to equilibrium in the initial state, and the change is consistent with the elevation feedback due to the lowered surface in the contracted margins. The area-mean ratio of changes in surface air temperature and surface elevation is 7.1 and $6.6 \, \mathrm{K \, km^{-1}}$ within the initial and

295   contracted ice-sheet extent respectively, close to the value of $6 \, \mathrm{K \, km^{-1}}$ assumed in the downscaling scheme. It is not uniform over the ice-sheet (Figure C1), but it is within in the range 4–8 $\mathrm{K \, km^{-1}}$ over more than half of the ice-sheet (considering either extent).

     The uncoupled ice-sheet is similarly located in the north of Greenland, but has larger area and lower altitude (Figure 3d1). Its specific SMB is negative *everywhere*, and its area-integral SMB is *more* negative than in the initial state, and $\sim$4 times

300   more than for the coupled ice-sheet (Figure 3d2). The much larger change exceeds the lapse-rate effect, and the area-mean specific SMB for any surface altitude above 1000 m is more negative in the uncoupled case than the coupled. The main cause is greater downwelling shortwave radiation at the surface in the uncoupled case (Figure 3c3,d3), due to lower cloud fraction. The region occupied by the contracted ice-sheet coincides geographically with the high cold interior of the initial ice-sheet, where cloudiness is comparatively low, but in the coupled case the cloudiness increases there as the ice-sheet becomes smaller

305   and lower, giving a powerful negative feedback on the mass-loss.

     In the coupled experiment, the precipitation from the south-west advances inland, following the the margin of the contracting ice-sheet (compare the grey contour line for $1 \, \mathrm{m \, yr^{-1}}$ in Figure 3b4,c4). Consequently the precipitation on the ice-sheet is about 15% greater in the coupled case. However, the snowfall is about 15% *less* in the coupled case (colours and numbers in Figure 3c4,d4), because its surface is lower than in the initial climate, making the surface climate warmer and reducing

310   the snowfall fraction (to 64%). The uncoupled SMB has a larger snowfall fraction (84%) because the surface in the region it occupies was initially much higher. The phase change of precipitation with elevation is omitted from the downscaling in the coupling scheme (as mentioned earlier); including it in the uncoupled model would reduce the snowfall, and make its SMB even more negative.

     In summary, the uncoupled ice-sheet is eliminated rapidly through the small ice-cap instability (elevation feedbacks from

315   surface energy fluxes and temperature), whereas in the coupled case the decline is decelerated, and the ice-sheet not completely elimated, owing to negative feedbacks of topographic change on regional climate (changes in cloudiness and precipitation). The comparison demonstrates the critical role of ice-sheet–climate interaction.

4.4   Final topography of the ice-sheet

According to the topographic features present, the final states can be put in five categories (indicated by symbols at the ends

320   of the trajectories in Figure 4b). In cases with small change in M, the final state is similar to the present day (configuration labelled "EWNS" *e.g.* Figure 3a1). The northern portion (denoted "N") is absent in some final states and the summit further south than in the present day *e.g.* Figure 3f1 (EWS). Ice in the south ("S") may become a separate ice-cap (as in Figure 3f1) or it may be absent, resembling Figure 3h1 (EWN) and 3g1 (EW). In cases with the smallest final M, the north-western lobe ("W")

vanishes, and ice remains only on the eastern mountains (E). For example, in the experiment ending in Figure 3e1 (marked with
325 "e" in Figure 4b), the southern and north-western domes detach and vanish within 3 kyr. Subsequently contraction continues
on all sides, but there is a slow small regrowth after the minimum mass is reached.

The transient and final states of all experiments lie close to a common power-law relationship between ice-sheet mass M
and area A with $M \propto A^{1.31}$ (Figure 2f), similar to the exponent of 1.36–1.38 derived for glaciers from observations and theory
(Bahr and Radić, 2012, and references therein). Final states with the same configuration have a characteristic deviation from
330 the common relationship *e.g.* EWN states have greater M.

Because of the elevation feedback, the mass-loss sometimes accelerates by a few tenths of a mm yr^{-1} SLE while one of the
outlying portions becomes separate or is eliminated, in a few cases after some millennia of relatively slow change. This is a
similar phenomenon to the saddle collapse during the separation of the Laurentide and Cordilleran ice-sheets during the last
deglaciation (Gregoire et al., 2012), but an order of magnitude smaller. For example, in the experiment ending in Figure 3f1
335 (the dotted green line, marked "f", in Figure 4b), the rate of ice loss accelerates after 10 kyr, at the start of the retreat of the
northern margin, which is completed by 15 kyr.

5 Non-existence of a threshold warming

In Section 2 we described why ΔSAT that reduces Greenland SMB to zero is expected to be a threshold warming beyond
which the ice-sheet would be eliminated. In Section 4 we found no evidence for a threshold from FiG results, meaning that the
340 conceptual basis for its existence is incorrect. The ice-sheet endures, albeit in a much reduced state, even for ΔSAT giving large
negative SMB, because the expected runaway feedback (the small ice-cap instability) does not occur. The positive feedbacks on
mass-loss due to reduction of thickness are weak, and overwhelmed by effects due to reduction of area. The conceptual model
considers that the smallest possible steady state has almost the same area as now, but in FiG most steady states have smaller
area. Because neither the initial specific SMB nor the change in it are geographically uniform, some parts of the ice-sheet can
345 be removed more readily.

In cases where specific SMB is initially positive, it becomes more positive (Figure 2e), because the areas from which the ice-
sheet retreats are predominantly those of relatively larger ablation or smaller snowfall. Consequently the area-integral SMB (the
product of increasing specific SMB and decreasing area) changes relatively little (fairly vertical trajectories in Figure 2b). For
instance, under MIROC5 RCP4.5 climate with medium albedo, the initial S, P and R are 150, 735 and 585 Gt yr^{-1} (Table 1).
350 The final S is the same as the initial because R and P both decrease by 115 Gt yr^{-1} (Figure 2f2,f4), a larger fractional decline
in R (20%) than in P (15%). The steady state is achieved by the withdrawal of the margin from the coast in some sectors,
reducing D sufficiently (by 209 Gt yr^{-1} or 60%) to balance the smaller S.

In cases where specific and area-integral SMB are initially negative, they become positive (Figure 2b,e). This happens
because P decreases less than R. For instance, under HadGEM2 abrupt4xCO2 climate with low albedo, the initial S, P and R
355 are -756, 797 and 1554 Gt yr^{-1} (Figure 2b2,b4). The final state is a small eastern ice-cap (like Figure 2e1 but smaller) with
S, P and R of 9, 31 and 21 Gt yr^{-1}; P is 3.9% and R 1.4% of the initial value. The ice-cap receives greater precipitation

17

and snowfall than the same region did initially (compare Figure 2b4,e4), and has more cloud and less surface downwelling shortwave (Figure 2b3,e3), because of the effect of topography on atmospheric circulation and climate.

6   Threshold for irreversible mass-loss

360   Greenland ice-sheet mass-loss in the first set of experiments occurs on timescales which are comparable with or even longer than those of surface climate change and natural CO_2 removal. We therefore also consider whether the ice-sheet mass would increase again if the climate cooled down. This will inform us about any irreversible commitment to GMSLR that might be incurred in coming decades despite subsequent CO_2 removal.

To study this question, we carry out a second set of FiG experiments, using MIROC5 1980-1999 BCs and recent CO_2,
365   starting from various transient and final steady states of the ice-sheet with reduced size from the first set of experiments. This is as if the climate instantaneously reverted to its late 20th century condition after many centuries in a high-CO_2 warm steady state, during which the ice-sheet had been losing mass. The second set includes experiments with all three choices of albedo. All but one of the experiments with medium albedo (solid green lines in Figure 4c) begin from states of various mass along the trajectory of the CanESM2 RCP8.5 medium-albedo experiment (green line with circles in Figure 4b), whose final steady-state
370   ice-sheet mass is 1.21 m SLE. All but one of those with low albedo (solid red lines in Figure 4c) begin from states of the HadGEM2-ES abrupt4xCO2 low-albedo experiment (red line with circles in Figure 4b), whose final mass of 0.12 m SLE is the smallest of all in the first set. The single high-albedo experiment in the second set (solid blue line in Figure 4c) also begins from this minimal state.

6.1   Regrown steady states

375   In the initial state of all the experiments of the second set, the ice-sheet has a smaller mass than present, and it grows to reach a new steady state; there are none in which it continues to lose mass (Figure 4c). However, the mass of the regrown steady state depends on the initial state and the albedo.

With high albedo, the ice-sheet regrows, in about 50 kyr, from the minimal state to a steady state with the extent of the present day's (EWNS configuration, Figure 4c). Since this starting state is a limiting case, we assume that the ice-sheet would
380   reach the same final state from any initial state, implying that this is only steady state for historical climate with high albedo. Therefore the loss of the ice-sheet would be reversible, albeit on a long timescale, if the high albedo is realistic.

On the other hand, with the medium and low albedo, two distinct sets of steady states can be reached in the second set of experiments, one set with final mass of 7 m SLE or more, the other with final mass of 5–6 m SLE. Initial states are divided between these two sets of final states by a threshold of initial mass at 4.0 m SLE with the medium albedo, and 3.9 m SLE with
385   the low albedo.

Starting above the threshold, the ice-sheet regrows to the EWNS configuration with medium albedo as with high (Figure 4c), but with low albedo there are two steady states. The larger is the EWNS configuration (7.3 m SLE, Figure 3a1), while the smaller lacks the southern dome (7.0 m SLE, EWN configuration, Figure 3h1). We will refer to these two configurations

together as WOWS ("with or without S"). The southern dome has positive SMB in the historical climate (Figure 3a2), but in

390 the warm climates it is readily lost due to increased ablation, and in the historical climate without the dome there is negative SMB inhibiting readvance at the new southern margin (Figure 3h2). The snowfall is however little changed in that region (Figures 3a4,h4). The southern dome is the last part of the ice-sheet to reappear with the high and medium albedoes (solid green and blue lines in Figure 4c after 30 kyr), and perhaps it would do so with low albedo after sufficiently long as well.

Starting below the threshold, the ice-sheet attains steady states lacking the northern portion, which we will refer to collec-

395 tively as NON states ("no N"). The steady state with medium albedo has the EWS configuration (5.7 m SLE, like Figure 3f1 in extent but thicker). With the low albedo, there are two steady states, having masses of 5.3 m SLE (EW configuration, Figure 3g1) and 5.0 m SLE (E configuration, like Figure 3e1 but much larger), which differ because the north-western dome is missing in the latter case. Again, we suppose this dome might regrow in time, given that it is the last part to do so with medium albedo.

400 Other authors have likewise found that the present state of the Greenland ice-sheet is not the only steady state under historical climate (Ridley et al., 2010; Solgaard and Langen, 2012; Robinson et al., 2012). A minimal state with ice solely or mostly in the east is a common feature of all these studies and ours. In other respects the steady-state configurations are dissimilar. The medium state of Robinson et al. (2012) most resembles our NON states. Our results are more complex than others in showing five steady states. We suppose that this is because greater detail in the interaction of the ice-sheet topography with atmospheric

405 circulation and SMB can be simulated by FAMOUS–ice than by the simpler approaches of previous studies.

6.2 Vulnerability of the ice-sheet to irreversible loss

To summarise our second set of experiments: transient states which have passed below the threshold regrow to NON steady states, while those still above the threshold regrow to WOWS steady states. Consistent with this, we note that all final states lying below the threshold in the first set of experiments are NON states (Figure 4b). States taken from below the threshold on

410 trajectories of rapid decline show no tendency for the northern portion to regrow, even after tens of millennia under historical climate. The difference between initial states just above and just below the threshold is infinitesimal, yet sufficient to perturb the climate and SMB such as to make them diverge radically in outcome through ice-sheet–climate feedback. The probable reason is that ablation exceeds accumulation in the northern region without the ice-sheet (shown by negative SMB at the northern margin in Figure 3g2), partly because snowfall is reduced (Figure 3a4,g4). Thus about 2 m of GMSLR will become

415 irreversible once the Greenland ice-sheet mass drops below the threshold, if the medium or low albedo is realistic.

The low- and medium-albedo NON steady states are 1–2 m SLE above the threshold, and yet grow no further, because they have lost the northern portion. This implies that, for states between the threshold mass (4 m SLE) and the NON mass (5–6 m SLE), the outcome depends on the history. To test this, we have conducted experiments (dashed lines in Figure 4c) beginning from the two steady states in this range (large circles at the end of dashed lines in Figure 4b), which were reached by slowly

420 declining trajectories. Initially the ice-sheet mass grows but, unlike when starting from rapidly declining transient states in this range, it soon becomes nearly constant at a slightly higher M than is reached from states below the threshold. This difference is due to a large southern dome in these cases, which was kept during the slow decline (along the dashed lines leading to the

large circles in Figure 4b) but had been lost already in states of the same mass in the warmer climate producing the fast decline (the solid lines with red and green circles in Figure 4b), and is not rebuilt in the historical climate. This result suggests that, for

425   slow or quasi-static decline of the ice-sheet, the NON mass itself is the threshold of irreversibility.

Using the linear relationship between the initial rate of mass-loss and the final steady-state mass in the first set of experiments (solid line in Figure 2d), we can translate the threshold ice-sheet mass (horizontal red and green lines) into a threshold on initial rate of loss (vertical red and green lines). Under a warm climate which initially gives a more negative ΔSMB than the threshold rate, the ice-sheet will eventually decline to a state which is smaller than the threshold mass. Roughly estimating a range from

430   the scatter in the relationship, the results suggest that the threshold ΔSMB lies between -500 and -150 Gt yr^{-1} (Figure 2d). Recent observed ΔSMB is at the upper end of this range (van den Broeke et al., 2016). Since the present-day rate of mass-loss is at the lower end of our scenarios, the relevant threshold may instead be the NON steady-state mass of about 5.5 m SLE (as suggested in the previous paragraph), in which case the linear fit indicates that the present ΔSMB is close to the threshold for partial irreversible loss of the ice-sheet.

435   If the present rate of mass-loss of about 0.7 mm yr^{-1} SLE persisted, it would take about 5000 years for the ice-sheet mass to reach the threshold of irreversibility, and 2500 years to reach the NON steady-state mass. At the highest rate of loss simulated in our experiments for the end of this century, of about 2 mm yr^{-1} SLE, it would take 1700 years to reach the threshold. Allowing for systematic uncertainty, the AR5 predicted even larger rates of mass-loss due to SMB perturbation, of up to about 6 mm yr^{-1} SLE by the end of the century, at which rate the threshold would be reached in 600 years.

440   In order to avoid eventual irreversible ice-loss, the climate must be returned to near pre-industrial before the threshold mass is reached. Reversing climate change requires extracting heat from the ocean, as well as removing the radiative forcing. If that can be done at all, it could not be done instantaneously, and mitigating climate change in the short term will buy more time to save the ice-sheet on the long term. Further simulations would be required to evaluate whether particular trajectories of future climate would avoid irreversible ice-loss.

445   # 7   Conclusions

We have studied the multimillennial future evolution of the Greenland ice-sheet in response to various magnitudes of anthropogenic climate change, in experiments with an AGCM interactively coupled to a dynamic ice-sheet model. For adequate resolution of gradients, especially at the margins of the ice-sheet, the surface mass balance is simulated by the AGCM as a function of elevation within its gridboxes. Our aim is not to produce time-dependent projections for coming centuries, but

450   instead to investigate the long-term consequences for global-mean sea-level rise (GMSLR).

Under climates that are warmer than the late 20th century, the ice-sheet loses mass, its surface elevation decreases and its surface climate becomes warmer. This gives a positive feedback on mass-loss, but it is outweighed by the negative feedbacks due to declining ablation area and increasing cloudiness over the interior as the ice-sheet contracts. Snowfall decreases less than ablation because the precipitation on the margins is enhanced by the topographic gradient, and moves inland as the ice-sheet

455   retreats. Consequently after many millennia under a constant warm climate the ice-sheet reaches a reduced steady state.

Contrary to expectation based on work using simpler climate models (Huybrechts et al., 1991; Gregory et al., 2004; Gregory and Huybrechts, 2006; Robinson et al., 2012; van den Broeke et al., 2016; Pattyn et al., 2018), we find no evidence for a threshold in Greenland or global warming that divides scenarios in which the ice-sheet suffers little reduction in its final steady state from those which it is mostly lost. We think that this difference arises from our using an AGCM, whose dynamics

460 and physical detail are needed to simulate the response of snowfall and cloudiness to the evolving topography. Support for this hypothesis comes from comparison with an experiment using the uncoupled ice-sheet model, in which the surface mass balance evolves only through the elevation feedback, and effects of atmospheric circulation change are omitted. In that case an almost constant rate of mass-loss is maintained for 3 kyr, during which the ice-sheet vanishes completely.

Under a warm climate, the final ice-sheet mass, and the entailed commitment to GMSLR, are well-correlated with the initial

465 perturbation to surface mass balance, and hence with the magnitude of climate change imposed. The final mass is also affected by the geographical pattern of climate change. If a climate like the present were maintained indefinitely, Greenland ice-sheet mass-loss would produce 1.5–2.5 m of GMSLR; with the climate of the RCP8.5 scenario for the late 21st century, the ice-sheet would be almost completely eliminated, with over 7 m of GMSLR.

When transient and steady states of the ice-sheet obtained under warm climates are transplanted into the late 20th century

470 climate, as if subsequent anthropogenic climate change had been reversed, the ice-sheet regrows in all cases, over tens of millennia, but not necessarily to its present-day size (as also found by Charbit et al., 2008; Ridley et al., 2010; Robinson et al., 2012). The resulting steady states can be put in two groups, according to whether ice is present in the northern part of the island. If the ice-sheet retreats from this region, it may not regrow, because the snowfall is reduced there, meaning that about 2 m of GMSLR would become irreversible. This threshold size might eventually be reached with the present-day climate, and would

475 be reached in about 600 years with the greatest rates of mass-loss projected for 2100 under RCP8.5 by Church et al. (2013). In order to avoid irreversible GMSLR, it would be necessary to restore the late 20th-century climate, in which the ice-sheet was near to mass balance, before the threshold is crossed.

The reliability of our conclusions depends on the realism of our model. There are systematic uncertainties arising from assumptions made in its formulation (for example, the uniform lapse rate and the omission of phase change of precipitation

480 in the downscaling). The snow albedo is a particularly important uncertainty; with our high choice of albedo, removal of the ice-sheet is reversible under present-day climate. Nonetheless, our results demonstrate the importance of climate–ice-sheet interaction to projecting the future of the Greenland ice-sheet. It would obviously be useful if similar investigations were done with other models that couple an ice-sheet to an atmosphere GCM (perhaps as components of an AOGCM or Earth system model). Even with a low-resolution GCM such as ours, long experiments are computationally demanding, meaning that our

485 results give only a sketchy outline of possible behaviour, and they could be supplemented by using an emulator to explore a wider range of scenarios (Edwards et al., 2019).

Appendix A: Relationship of albedo to steady-state historical M

490 Continuing the spinup experiments (which are among the experiments of Section 4), M remains at 7.7 m SLE with low albedo, with medium albedo it declines slightly to a steady state of 7.4 m SLE (very close to observed) over about 10 kyr, and with low albedo to 7.1 m SLE over 15 kyr (Figure A1). These are small changes compared with those simulated for 21st-century climate change (Section 4). Nonetheless, these small differences in M for low and high albedo from observations show that requiring a a realistic steady state of the ice-sheet in a coupled model provides a strong constraint on the SMB simulation to

495 which regional climate models such as MAR and RACMO are not subjected. A quadratic fit to the relationship between SMB and M in FiG steady states with MIROC5 historical climate gives $M = 7.9$ m SLE for the SMB of 437 Gt yr^{-1} simulated by MAR for this climate.

An even higher choice of albedo in FiG gave SMB of 610 Gt yr^{-1} and a steady-state M of 8.2 m SLE, and an even lower choice 195 Gt yr^{-1} with M tending towards a steady state substantially below 7.0 m. These values of SMB approximately

500 bound the range of SMB variations in the 20th century reconstructed with MAR (Fettweis et al., 2017, their Figure 8a), indicating that they could plausibly occur with historical climate and the present-day ice-sheet topography (as in MAR), but we excluded those choices of albedo because they would not be consistent with realistic M.
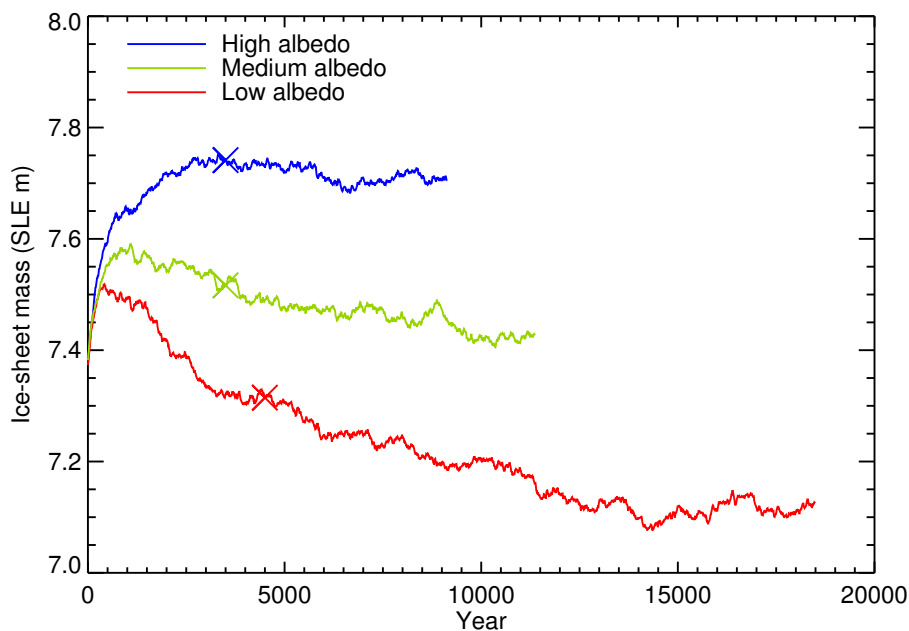

Figure A1. Timeseries of Greenland ice-sheet mass with constant climate for 1980–1999 simulated by MIROC5 during FiG spinup integrations beginning from the observed topography (Bamber et al., 2001a, b). The crosses indicate the states from which the experiments of Section 4 were initiated.

Appendix B: Alternatives to ΔSAT

In Figure 2 we obtain global-mean annual-mean surface air temperature change ΔSAT from FAMOUS–ice. It may also be obtained from the AOGCMs that supply the sea-surface BCs. This is almost the same (Figure B1a). They differ because surface air temperature is not prescribed over land from the BCs in FAMOUS–ice.

We have investigated two other measures of temperature change but neither is a better predictor than ΔSAT for the final M (Figure B1c,d).
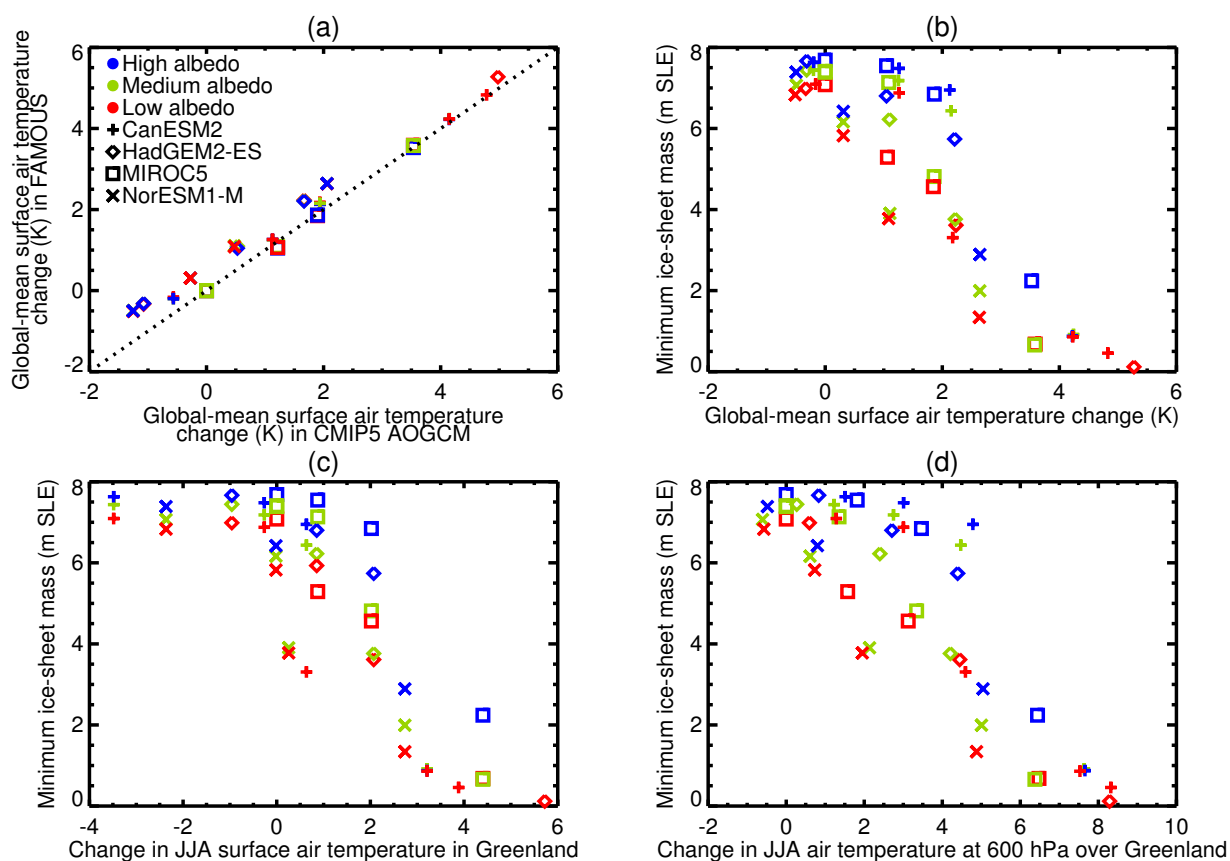

Figure B1. (a) Relationship between global-mean annual-mean surface air temperature change in FAMOUS–ice AGCM experiments and in the portions of the CMIP5 AOGCM experiments used to supply the FAMOUS–ice SST boundary conditions; (b,c,d) Relationships of ΔSMB to (b) FAMOUS–ice global-mean annual-mean SAT change (the same as Figure 2c and repeated here for comparison), (c) FAMOUS–ice Greenland area-mean summer-mean (JJA) SAT change, (d) FAMOUS–ice area-mean summer-mean air temperature change at 600 hPa over Greenland. Changes are computed from the first 300 ice-sheet years of each FAMOUS–ice experiment and expressed relative to the MIROC5 historical climate with the same albedo parameter.

Appendix C: Lapse rate

510   In the downscaling of surface air temperature from FAMOUS gridboxes to FAMOUS–ice elevation tiles, we assume a uniform lapse rate of 6 K km^{-1}. Consequently this lapse rate is also used to predict the derivative of surface air temperature with respect to elevation change when Glimmer is run uncoupled from the AGCM. The derivative diagnosed from the coupled experiment is shown in Figure C1.
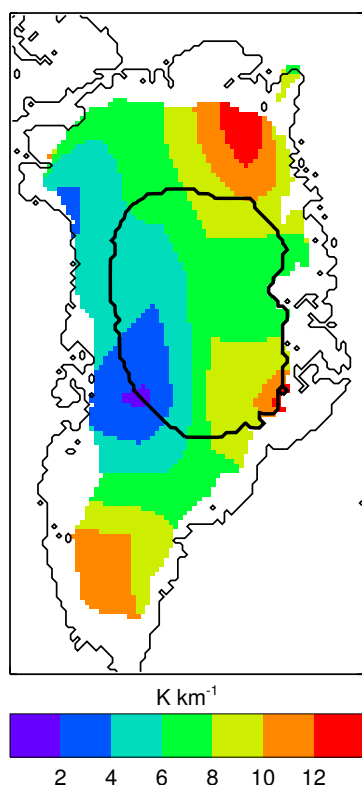
Figure C1. Change in surface air temperature divided by change in surface altitude (K km^{-1}) in the difference between the initial state of the experiment with HadGEM2-ES abrupt4xCO2 climate and low albedo and the state after 3600 years (Figures 3b1,c1). The thick black line is the ice-sheet edge in the latter state.

Author contributions. SEG and RSS developed the model, SEG and JMG ran the experiments, JMG carried out the analysis and wrote the
515   paper.

References

520 Aschwanden, A., Fahnestock, M. A., Truffer, M., Brinkerhoff, D. J., Hock, R., Khroulev, C., Mottram, R., and Khan, S. A.: Contribution of the Greenland ice sheet to sea level over the next millennium, Sci. Adv., 5, eaav9396, https://doi.org/10.1126/sciadv.aav9396, 2019.

Bahr, D. B. and Radić, V.: Significant contribution to total mass from very small glaciers, The Cryosphere, 6, 763–770, https://doi.org/10.5194/tc-6-763-2012, 2012.

Bamber, J., Layberry, R. L., and Gogenini, S. P.: A new ice thickness and bed data set for the Greenland ice sheet 1: Measurement, data

525 reduction, and errors, J. Geophys. Res., 106, 33 773–33 780, https://doi.org/10.1029/2001JD900054, 2001a.

Bamber, J. L., Ekholm, S., and Krabill, W. B.: A new, high-resolution digital elevation model of Greenland fully validated with airborne laser altimeter data, J. Geophys. Res., 106, 6733–6745, https://doi.org/10.1029/2000JB900365, 2001b.

Bamber, J. L., Westaway, R. M., Marzeion, B., and Wouter, B.: The land ice contribution to sea level during the satellite era, Environ. Res. Lett., 13, 063 008, https://doi.org/10.1088/1748-9326/aac2f0, 2018.

530 Charbit, S., Paillard, D., and Ramstein, G.: Amount of CO_2 emissions irreversibly leading to the total melting of Greenland, Geophys. Res. Lett., 35, https://doi.org/10.1029/2008GL033472, 2008.

Church, J. A., Clark, P. U., Cazenave, A., Gregory, J. M., Jevrejeva, S., Levermann, A., Merrifield, M. A., Milne, G. A., Nerem, R. S., Nunn, P. D., Payne, A. J., Pfeffer, W. T., Stammer, D., and Unnikrishnan, A. S.: Sea Level Change, in: Climate Change 2013: The Physical Science Basis. Contribution of Working Group I to the Fifth Assessment Report of the Intergovernmental Panel on Climate Change,

535 edited by Stocker, T. F., Qin, D., Plattner, G.-K., Tignor, M., Allen, S. K., Boschung, J., Nauels, A., Xia, Y., Bex, V., and Midgley, P. M., Cambridge University Press, https://doi.org/10.1017/CBO9781107415324.026, 2013.

Clark, P. U., Shakun, J. D., Marcott, S. A., Mix, A. C., Eby, M., Kulp, S., Levermann, A., Milne, G. A., Pfister, P. L., Schrag, B. D. S. D. P., Solomon, S., Stocker, T. F., Strauss, B. H., Weaver, A. J., Winkelmann, R., Archer, D., Bard, E., Goldner, A., Lambeck, K., Pierrehumbert, R. T., and Plattner, G.-K.: Consequences of twenty-first-century policy for multi-millennial climate and sea-level change, Nature Climate

540 Change, 6, 360–369, https://doi.org/10.1038/NCLIMATE2923, 2016.

Edwards, T. L., Fettweis, X., Gagliardini, O., Gillet-Chaulet, F., Goelzer, H., Gregory, J. M., Hoffman, M., Huybrechts, P., Payne, A. J., Perego, M., Price, S., Quiquet, A., and Ritz, C.: Effect of uncertainty in surface mass balance–elevation feedback on projections of the future sea level contribution of the Greenland ice sheet, The Cryosphere, 8, 195–208, https://doi.org/10.5194/tc-8-195-2014, 2014.

Edwards, T. L., Brandon, M. A., Durand, G., Edwards, N. R., Golledge, N. R., Holden, P. B., Nias, I. J., Payne, A. J., 3, C. R., and Wernecke,

545 A.: Revisiting Antarctic ice loss due to marine ice-cliff instability, Nature, 566, 58–64, https://doi.org/10.1038/s41586-019-0901-4, 2019.

Fettweis, X., Franco, B., Tedesco, M., van Angelen, J. H., Lenaerts, J. T. M., van den Broeke, M. R., and Gallée, H.: Estimating the Greenland ice sheet surface mass balance contribution to future sea level rise using the regional atmospheric climate model MAR, The Cryosphere, 7, 469–489, https://doi.org/10.5194/tc-7-469-2013, 2013.

Fettweis, X., Box, J. E., Agosta, C., Amory, C., Kittel, C., Lang, C., van As, D., Machguth, H., and Gallée, H.: Reconstructions of

550 the 1900–2015 Greenland ice sheet surface mass balance using the regional climate MAR model, The Cryosphere, 11, 1015–1033, https://doi.org/10.5194/tc-11-1015-2017, 2017.

Fürst, J. J., Goelzer, H., and Huybrechts, P.: Ice-dynamic projections of the Greenland ice sheet in response to atmospheric and oceanic warming, The Cryosphere, 9, 1039–1062, https://doi.org/10.5194/tc-9-1039-2015, 2015.

Golledge, N. R., , Keller, E. D., Gomez, N., Naughten, K. A., Bernales, J., Trusel, L. D., and Edwards, T. L.: Global environmental conse-

555 quences of twenty-first-century ice-sheet melt, Nature, 566, 65–72, https://doi.org/10.1038/s41586-019-0889-9, 2019.

Gordon, C., Cooper, C., Senior, C. A., Banks, H., Gregory, J. M., Johns, T. C., Mitchell, J. F. B., and Wood, R. A.: The Simulation of SST, sea ice extents and ocean heat transports in a version of the Hadley Centre coupled model without flux adjustments, Clim. Dyn., 16, 147–168, https://doi.org/10.1007/s003820050010, 2000.

Gregoire, L. J., Payne, A. J., and Valdes, P. J.: Deglacial rapid sea level rises caused by ice-sheet saddle collapses, Nature, 487, 219–223, https://doi.org/10.1038/nature11257, 2012.

Gregory, J. M. and Huybrechts, P.: Ice-sheet contributions to future sea-level change, Philos. Trans. R. Soc. London, 364, 1709–1731, https://doi.org/10.1098/rsta.2006.1796, 2006.

Gregory, J. M., Huybrechts, P., and Raper, S. C. B.: Threatened loss of the Greenland ice-sheet, Nature, 428, 616, 2004.

Gregory, J. M., Browne, O. J. H., Payne, A. J., Ridley, J. K., and Rutt, I. C.: Modelling large-scale ice-sheet–climate interactions following glacial inception, Clim. Past, 8, 1565–1580, https://doi.org/10.5194/cp-8-1565-2012, 2012.

Gregory, J. M., Bouttes, N., Griffies, S. M., Haak, H., Hurlin, W. J., Jungclaus, J., Kelley, M., Lee, W. G., Marshall, J., Romanou, A., Saenko, O. A., Stammer, D., and Winton, M.: The Flux-Anomaly-Forced Model Intercomparison Project (FAFMIP) contribution to CMIP6: investigation of sea-level and ocean climate change in response to CO_2 forcing, Geosci. Model Devel., 9, 3993–4017, https://doi.org/10.5194/gmd-9-3993-2016, 2016.

Hanna, E., Mernild, S. H., Cappelen, J., and Steffen, K.: Recent warming in Greenland in a long-term instrumental (1881–2012) climatic context: I. Evaluation of surface air temperature records, Environ. Res. Lett., 7, 045 404, https://doi.org/10.1088/1748-9326/7/4/045404, 2012.

Hofer, S., Tedstone, A. J., Fettweis, X., and Bamber, J. L.: Decreasing cloud cover drives the recent mass loss on the Greenland ice sheet, Sci. Adv., 3, e1700 584, https://doi.org/10.1126/sciadv.1700584, 2017.

Holland, D. M., Thomas, R. H., De Young, B., Ribergaard, M. H., and Lyberth, B.: Acceleration of Jakobshavn Isbrae triggered by warm subsurface ocean waters, Nature Geosci., 1, 659–664, https://doi.org/10.1038/ngeo316, 2008.

Huybrechts, P., Letreguilly, A., and Reeh, N.: The Greenland ice sheet and greenhouse warming, Palaeogeogr. Palaeocl., 89, 399–412, 1991.

Levermann, A., Clark, P. U., Marzeion, B., Milne, G. A., Pollard, D., Radic, V., and Robinson, A.: The multimillennial sea-level commitment of global warming, Proc. Natl. Acad. Sci. USA, 110, 13 745–13 750, https://doi.org/10.1073/pnas.1219414110, 2013.

Meehl, G. A., Stocker, T. F., Collins, W. D., Friedlingstein, P., Gaye, A. T., Gregory, J. M., Kitoh, A., Knutti, R., Murphy, J. M., Noda, A., Raper, S. C. B., Watterson, I. G., Weaver, A. J., and Zhao, Z.: Global climate projections, in: Climate Change 2007: The Physical Science Basis. Contribution of Working Group I to the Fourth Assessment Report of the Intergovernmental Panel on Climate Change, edited by Solomon, S., Qin, D., Manning, M., Chen, Z., Marquis, M., Averyt, K. B., Tignor, M., and Miller, H. L., Cambridge University Press, 2007.

Mouginot, J., Rignot, E., Bjørk, A. A., van den Broeke, M., Millan, R., Morlighem, M., Noël, B., Scheuchl, B., and Wood, M.: Forty-six years of Greenland Ice Sheet mass balance from 1972 to 2018, Proc. Natl. Acad. Sci. USA, 19, 9239–9244, https://doi.org/10.1073/pnas.1904242116, 2019.

Nick, F. M., Vieli, A., Andersen, M. L., Joughin, I., Payne, A., Edwards, T. L., Pattyn, F., and van de Wal, R. S. W.: Future sea-level rise from Greenland's main outlet glaciers in a warming climate, Nature, 497, 235–238, https://doi.org/10.1038/nature12068, 2013.

Noël, B., van de Berg, W. J., van Wessem, J. M., van Meijgaard, E., van As, D., Lenaerts, J. T. M., Lhermitte, S., Kuipers Munneke, P., Smeets, C. J. P. P., van Ulft, L. H., van de Wal, R. S. W., and van den Broeke, M. R.: Modelling the climate and surface mass balance of polar ice sheets using RACMO2—Part 1: Greenland (1958–2016), The Cryosphere, 12, 811–831, https://doi.org/10.5194/tc-12-811-2018, 2018.

Pattyn, F., Ritz, C., Hanna, E., Asay-Davis, X., DeConto, R., Favier, G. D. L., Fettweis, X., Goelzer, H., 0, N. R. G., Munneke, P. K., Lenaerts,
J. T. M., Nowicki, S., Payne, A. J., Seroussi, A. R. H., Trusel, L. D., and van den Broeke, M.: The Greenland and Antarctic ice sheets
under 1.5°C global warming, Nature Climate Change, 8, 1053–1061, https://doi.org/10.1038/s41558-018-0305-8, 2018.

Ridley, J., Huybrechts, P., Gregory, J. M., and Lowe, J. A.: Elimination of the Greenland ice sheet in a high CO_2 climate, J. Climate, 18,
3409–3427, https://doi.org/10.1175/JCLI3482.1, 2005.

Ridley, J., Gregory, J. M., Huybrechts, P., and Lowe, J.: Thresholds for irreversible decline of the Greenland ice sheet, Clim. Dyn., 35,
1065–1073, https://doi.org/10.1007/s00382-009-0646-0, 2010.

Roberts, W. H. G., Valdes, P. J., and Payne, A.: Topography's crucial role in Heinrich events, Proc. Natl. Acad. Sci. USA, 111, 16 688–16 693,
https://doi.org/10.1073/pnas.1414882111, 2014.

Robinson, A., Calov, R., and Ganopolski, A.: Greenland ice sheet model parameters constrained using simulations of the Eemian Interglacial,
Clim. Past, 7, 381–396, https://doi.org/10.5194/cp-7-381-2011, 2011.

Robinson, A., Calov, R., and Ganopolski, A.: Multistability and critical thresholds of the Greenland ice sheet, Nature Climate Change, 2,
429–432, https://doi.org/10.1038/NCLIMATE1449, 2012.

Rückamp, M., Falk, U., Frieler, K., Lange, S., and Humbert, A.: The effect of overshooting 1.5°C global warming on the mass loss of the
Greenland ice sheet, Earth Syst. Dynam., 9, 1169–1189, https://doi.org/10.5194/esd-9-1169-2018, 2018.

Rutt, I. C., Hagdorn, M., Hulton, N. R. J., and Payne, A. J.: The Glimmer community ice sheet model, J. Geophys. Res., 114, F02 004,
https://doi.org/10.1029/2008JF001015, 2009.

Shepherd, A., Ivins, E. R., A, G., Barletta, V. R., Bentley, M. J., Bettadpur, S., Briggs, K. H., Bromwich, D. H., Forsberg, R., Galin, N.,
Horwath, M., Jacobs, S., Joughin, I., King, M. A., Lenaerts, J. T. M., Li, J., Ligtenberg, S. R. M., Luckman, A., Luthcke, S. B., McMillan,
M., Meister, R., Milne, G., Mouginot, J., Muir, A., Nicolas, J. P., Paden, J., Payne, A. J., Pritchard, H., Rignot, E., Rott, H., Søorensen,
L. S., Scambos, T. A., Scheuchl, B., Schrama, E. J. O., Smith, B., Sundal, A. V., van Angelen, J. H., van de Berg, W. J., van den Broeke,
M. R., Vaughan, D. G., Velicogna, I., , Wahr, J., Whitehouse, P. L., Wingham, D. J., Yi, D., Young, D., and Zwally, H. J.: A Reconciled
Estimate of Ice-Sheet Mass Balance, Science, 338, 1183–1189, https://doi.org/10.1126/science.1228102, 2012.

Shepherd, A., Ivins, E., Rignot, E., Smith, B., van den Broeke, M., Velicogna, I., Whitehouse, P., Briggs, K., Joughin, I., Krinner, G., Nowicki,
S., Payne, T., Scambos, T., Schlegel, N., Geruo, A., Agosta, C., Ahlstrøm, A., Babonis, G., Barletta, V. R., Bjørk, A. A., Blazquez, A.,
Bonin, J., Colgan, W., Csatho, B., Cullather, R., Engdahl, M. E., Felikson, D., Fettweis, X., Forsberg, R., Hogg, A. E., Gallee, H., Gardner,
A., Gilbert, L., Gourmelen, N., Groh, A., Gunter, B., Hanna, E., Harig, C., Helm, V., Horvath, A., Horwath, M., Khan, S., Kjeldsen, K. K.,
Konrad, H., Langen, P. L., Lecavalier, B., Loomis, B., Luthcke, S., McMillan, M., Melini, D., Mernild, S., Mohajerani, Y., Moore, P.,
Mottram, R., Mouginot, J., Moyano, G., Muir, A., Nagler, T., Nield, G., Nilsson, J., Noël, B., Otosaka, I., Pattle, M. E., Peltier, W. R.,
Pie, N., Rietbroek, R., Rott, H., Sørensen, L. S., Sasgen, I., Save, H., Scheuchl, B., Schrama, E., Schröder, L., Seo, K.-W., Simonsen,
S. B., Slater, T., Spada, G., Sutterley, T., Talpe, M., Tarasov, L., Jan van de Berg, W., van der Wal, W., van Wessem, M., Vishwakarma,
B. D., Wiese, D., Wilton, D., Wagner, T., Wouters, B., and Wuite, J.: Mass balance of the Greenland Ice Sheet from 1992 to 2018, Nature,
https://doi.org/10.1038/s41586-019-1855-2, in press.

Smith, R. S.: The FAMOUS climate model (versions XFXWB and XFHCC): description update to version XDBUA, Geosci. Model Devel.,
5, 269–276, https://doi.org/10.5194/gmd-5-269-2012, 2012.

Smith, R. S., Osprey, A., and Gregory, J. M.: A description of the FAMOUS (version XDBUA) climate model and control run, Geosci. Model
Devel., 1, 53–68, https://doi.org/10.5194/gmd-1-53-2008, 2008.

Smith, R. S., George, S., and Gregory, J. M.: FAMOUS version sgfjb (FAMOUS-ice): energy- and water-conserving coupling with ice sheet models, in preparation.

Solgaard, A. M. and Langen, P. L.: Multistability of the Greenland ice sheet and the effects of an adaptive mass balance formulation, Clim. Dyn., 39, 1599–1612, https://doi.org/10.1007/s00382-012-1305-4, 2012.

635 Solgaard, A. M., Bonow, J. M., Langen, P. L., Japsen, P., and Hvidberg, C. S.: Mountain building and the initiation of the Greenland Ice Sheet, Palaeogeogr. Palaeocl., 392, 161–176, https://doi.org/10.1016/j.palaeo.2013.09.019, 2013.

Stouffer, R. J., Yin, J., Gregory, J. M., Dixon, K. W., Spelman, M. J., Hurlin, W., Weaver, A. J., Eby, M., Flato, G. M., Hasumi, H., Hu, A., Jungclaus, J., Kamenkovich, I. V., Levermann, A., Montoya, M., Murakami, S., Nawrath, S., Oka, A., Peltier, W. R., Robitaille, D. Y., Sokolov, A., Vettoretti, G., and Weber, N.: Investigating the Causes of the Response of the Thermohaline Circulation to Past and Future

640 Climate Changes, J. Climate, 19, 1365–1387, https://doi.org/10.1175/JCLI3689.1, 2006.

Tedesco, M., Fettweis, X., Mote, T., Wahr, J., Alexander, P., Box, J. E., and Wouters, B.: Evidence and analysis of 2012 Greenland records from spaceborne observations a regional climate model and reanalysis data, The Cryosphere, 7, 615–630, https://doi.org/10.5194/tc-7-615-2013, 2013.

Tedesco, M., Doherty, S., Fettweis, X., Alexander, P., Jeyaratnam, J., and Stroeve, J.: The darkening of the Greenland ice sheet: trends,

645 drivers, and projections (1981–2100), The Cryosphere, 10, 477–496, https://doi.org/10.5194/tc-10-477-2016, 2016.

Toniazzo, T., Gregory, J. M., and Huybrechts, P.: Climatic impact of a Greenland deglaciation and its possible irreversibility, J. Climate, 17, 21–33, 2004.

Trusel, L. D., Das, S. B., Osman, M. B., Evans, M. J., Smith, B. E., Fettweis, X., McConnell, J. R., Noël, B. P. Y., and van den Broeke, M. R.: Nonlinear rise in Greenland runoff in response to post-industrial Arctic warming, Nature, 564, 104–108, https://doi.org/10.1038/s41586-

650 018-0752-4, 2018.

van Angelen, J. H., Lenaerts, J. T. M., van den Broeke, M. R., Fettweis, X., and van Meijgaard, E.: Rapid loss of firn pore space accelerates 21st century Greenland mass loss, Geophys. Res. Lett., 40, 2109–2113, https://doi.org/10.1002/grl.50490, 2013.

van den Broeke, M. R., Enderlin, E. M., Howat, I. M., Kuipers Munneke, P., Noël, B. P. Y., van de Berg, W. J., van Meijgaard, E., , and Wouters, B.: On the recent contribution of the Greenland ice sheet to sea level change, The Cryosphere, 10, 1933–1946,

655 https://doi.org/10.5194/tc-10-1933-2016, 2016.

van Vuuren, D. P., Edmonds, J., Kainuma, M., Riahi, K., Thomson, A., Hibbard, K., Hurtt, G. C., Kram, T., Krey, V., Lamarque, J.-F., Masui, T., Meinshausen, M., Nakicenovic, N., Smith, S. J., and Rose, S. K.: The representative concentration pathways: an overview, Clim. Change, 109, 5–37, 2011.

Vizcaíno, M.: Ice sheets as interactive components of Earth System Models: progress and challenges, WIREs Climate Change,

660 https://doi.org/10.1002/wcc.285, 2014.

Vizcaíno, M., Mikolajewicz, U., Jungclaus, J., and Schurgers, G.: Climate modification by future ice sheet changes and consequences for ice sheet mass balance, Clim. Dyn., 34, 301–324, https://doi.org/10.1007/s00382-009-0591-y, 2010.

Vizcaíno, M., Lipscomb, W. H., Sacks, W. J., van Angelen, J. H., Wouters, B., and van den Broeke, M. R.: Greenland Surface Mass Balance as Simulated by the Community Earth System Model. Part I: Model Evaluation and 1850–2005 Results, J. Climate, 26, 7793–7812,

665 https://doi.org/10.1175/JCLI-D-12-00615.1, 2013.

Vizcaíno, M., Lipscomb, W. H., Sacks, W. J., and van den Broeke, M.: Greenland surface mass balance as simulated by the Community Earth System Model. Part II: Twenty-first-century changes, J. Climate, 27, 215–226, https://doi.org/10.1175/JCLI-D-12-00588.1, 2014.